CHEMISTRY OF MATERIALS

pubs.acs.org/cm

Article

Collagen-Targeted Theranostic Nanosponges for Delivery of the Matrix Metalloproteinase 14 Inhibitor Naphthofluorescein

Ting-Yi Wang, Laken L. Kendrick-Williams, Mei Y. Choy, Kelly A. Gilmore, Thomas Bonnard, Hannah A. Pearce, Lok Soon Law, Iska Carmichael, Stephen H. Cody, Karen Alt, Christoph E. Hagemeyer,* and Eva Harth*

Cite This: *Chem. Mater.* 2020, 32, 3707−3714

Read Online

ACCESS | Metrics & More | Article Recommendations | Supporting Information

ABSTRACT: We report the development of a theranostic collagen targeted cell penetrating drug delivery system toward treatment of cardiovascular disease. Caused by the action of matrix metalloproteinases (MMP), degraded collagen is a hallmark of unstable atherosclerotic plaques that are highly susceptible toward rupture. Targeting unstable plaques and delivering MMP blockers directly to plaque to inhibit MMP activity is a promising new strategy that requires the benefits and possibilities of nanodelivery approaches. The presented delivery system is designed to (a) target and bind to a cryptic epitope on collagen IV exposed through the degradative action of matrix metalloproteinase 2 (MMP2), (b) to image the targeting and cell uptake, and (c) to deliver the MMP14 inhibitor naphthofluorescein. In detail, the novel targeting unit is composed of a collagen-homing T-peptide and bound to a MMP2-cleavable activatable cell penetrating peptide (ACPP) which upon cleavage by MMP2 deposits the MMP14 blocker drug into cells, directly into contact with MMP 14 activating enzymes. To selectively attach both the targeting peptide and a reporting imaging dye, a nanosponge nanoparticle network is modified to present orthogonal aldehyde and thiol functional groups as surface units. The MMP14 inhibitor naphthofluorescein is loaded into the nanoparticle delivery system after postconjugation chemistries and finalizes the synthesis of this novel theranostic delivery system. The ability to evade phagocytosis is confirmed *in vitro* by using murine RAW cell line and effective cell uptake *in vitro* by using the MMP2 producing the HT1080 cell line is demonstrated. In this work, we have combined a highly specific targeting peptide directed against degraded collagen and a tailorable nanosystem that is deemed to deliver its potent drug load directly into cells, to inhibit the cascade for MMP activation which breaks down collagen structures leading to plaque rupture, the underlying cause of myocardial infarction and strokes.

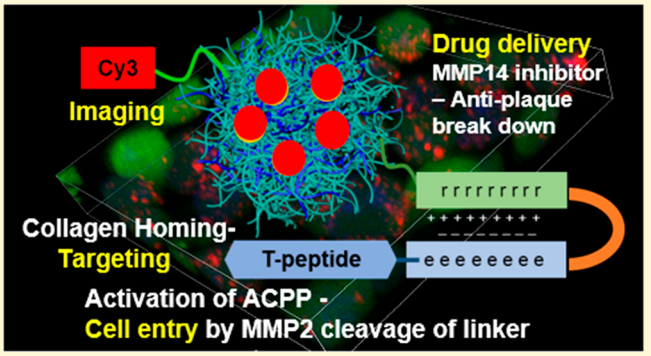

Cardiovascular disease is a major health burden and leading cause of mortality and morbidity in developed countries.[1] It is associated with atherosclerosis, or thickening of artery walls as a result of the accumulation of calcium and fatty materials. Unstable plaque rupture in a major coronary artery is responsible for more than two-thirds of fatal myocardial infarctions.[2]

One possibility to develop efficient therapies to stabilize the plaque is to suppress the activity of plaque matrix metalloproteinase (MMP). MMP activity has been associated with reduced collagen content[3] of plaques with thin, rupture-prone fibrous caps.[4] MMP14, a membrane type MMP, has been associated with unstable plaques[5] and plays a pivotal role in activating collagen degradative activity of several other MMPs, such as MMP2[6] and MMP9.[7] Previous human trials that systemically delivered broad spectrum MMP inhibitors, potentially targeting all 23 groups of MMPs, produced unacceptable side effects from indiscriminate MMP inhibition and off-site effects.[8,9] The limitation with broad spectrum inhibition of MMPs in atherosclerotic plaques stems from a current incomplete understanding of the roles of MMPs in plaque stability.[10] MMP14, MMP2, and MMP9 have been studied previously and associated with plaque instability, but other MMPs are believed to be potentially beneficial for stable plaque remodelling.[11] Consequently, there is an urgent need to deliver specific MMP blockers directly into the unstable plaque. Tailored nanomedicine in the form of targeted smart delivery nanoparticles has significant potential for this purpose with the goal to specifically deliver large quantities of drugs

Received: July 23, 2019
Revised: April 13, 2020
Published: April 14, 2020

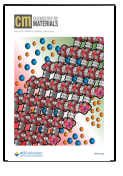

over a prolonged period of time, potentially providing long-term protections from plaque rupture.[12−17]

Advantages of biodegradable polymeric nanoparticles for drug delivery include the ability to formulate insoluble pharmaceutical agents and to improve the bioavailability of therapeutics.[18−21] Studies indicate that physical characteristics including nanoparticle size influence biological interactions, such as cell trafficking and accumulation,[22,24] and the ability to control the nanoscopic size range is therefore one of the critical parameters to develop viable candidates for drug delivery applications.[25−27] For example, 200 nm particles with narrow distribution can take advantage of the enhanced permeation and retention (EPR) effect,[28] and nanoparticles of 60−80 nm in size have shown optimum cell uptake and sustained retention time.[22,29] For the presented work, we selected a polyester based nanosponge delivery system. It showed in previous applications a high targeting ability toward cancer cell lines and an increased bioavailability of cancer therapeutics and could be produced in a nanoscopic range of ∼100 nm.[30,31] Another reason for the selection of the nanosponge delivery system was due to the ease of the targeting peptide attachment and the postloading with drugs after post modification of the carrier.[32−35] In addition, the particle release kinetics can be tailored for long-term drug delivery to enable a constant suppression of MMP degrading activity and to give the vessel time to recover. The implementation of these nanosponges as a targeted theranostic nanocarrier utilizing peptide homing to deliver a drug with specific MMP inhibition into atherosclerotic plaques is envisioned to have advantages over systemic approaches and to reduce off-target side effects, increase drug bioavailability at target sites, and reduce drug administration frequencies. In this contribution, we report the synthesis and proof-of-concept experiments of a peptide-conjugated, dye-labeled nanosponge loaded with a specific MMP14 inhibitor drug for the targeting and delivery to MMP degraded collagen and demonstrate the successful uptake into MMP2 producing macrophages (RAW cells) both found abundantly in unstable atherosclerotic plaques.

EXPERIMENTAL SECTION

Materials. All reagents, chemicals, antibodies, and solvents were purchased by Bio-Rad (Hercules, CA), EMD Millipore Cooperation (Billerica, MA), Fisher Chemicals (Princeton, NJ), R&D Systems (Minneapolis, MN), Invitrogen (Carlsbad, CA) Merck (Branchburg,NJ), Pierce (Rockford, IL), and Sigma-Aldrich (St. Louis, MO) and were used per the manufacturer's instructions. Other consumables were from the following commercial sources: Eppendorf (Westbury, NY), BD Bioscience (Bedford, MA), and ThermoScientific (Waltham, MA). Buffers and solutions were prepared per standard protocols.

Methods. *Synthesis of T-Peptide_ACPP.* H-Cys-2Cl-Trt-Cl-Resin was allowed to swell in dichloromethane (DCM) and then dried *in vacuo*. The first Fmoc-protected amino acid and 2-(1*H*-benzotriazole-1-yl)-1,1,3,3-tetramethyluronium hexafluorophosphate were dissolved in dimethylformamide (DMF) and added to the resin *N*-methylmorpholine (NMM). The resin was agitated by using a stream of N_2. The reaction solution was removed from the resin by suction, and the resin was washed with DMF. To perform the Kaiser test, a small amount of resin was placed in a test tube, and the Kaiser test solution was added. The resin solution was heated to 110 °C for 3 min. For Fmoc deprotection, the resin was treated with the deprotection solution during agitation by a N_2 stream, then washed with DMF, and dried *in vacuo*. This procedure was repeated for each amino acid in the peptide sequence. For the final wash, the resin was rinsed with methanol (MeOH), DCM, and then MeOH and dried *in vacuo* for 12 h prior to cleavage. A mixture of resin and cleavage solution was placed on a shaker table at 25 °C for 2 h. The resultant cleavage solution was filtered to remove the resin. To the filtrate, diethyl ether was added while stirring to precipitate the crude peptide. The ether mixture was centrifuged, and the supernatant was decanted. The peptide was washed with fresh ether and centrifuged again, and the supernatant was discarded. The crude peptide was collected as a white powder and dried *in vacuo* for 24 h. Final purification was performed by HPLC and characterized by MS (Figure S6).

Synthesis of the SHIP Probe. The following SHIP constructs were synthesized by Integrated DNA Technologies, Inc., with the indicated properties and the azido compound conjugated to the ACPP with Cu-catalyzed click chemistry. Purification was performed by HPLC.

Synthesis of Linear Poly(δ-valerolactone-co-α-allylvalerolactone). A 25 mL round-bottom flask equipped with a stir bar was flame-dried and purged with N_2 followed by addition of tin trifluoromethanesulfonate ($Sn(OTf)_2$). Isoamyl alcohol and DCM were added to the flask, and α-allyl-δ-valerolactone and δ-valerolactone, purified through vacuum distillation, were added sequentially and stirred at room temperature. The polymerization was quenched via addition of excess MeOH and then precipitated into cold MeOH to produce a white solid and dried under vacuum (50% yield). VL: 90.78%; AVL: 9.22%; $M_{n,NMR}$: 3165.75 g mol^{-1}. In step 2, the poly(VL-AVL) (200 mg, 63.2 mmol, 117.6 mmol of allyl) was dissolved in DCM and mixed with *m*-chloroporoxybenzoic acid dissolved in DCM. The reaction stirred at room temperature. The organic layer was washed with saturated sodium bicarbonate ($NaHCO_3$) solution and then dried over magnesium sulfate. The polymer was dried under vacuum to collect a white waxy solid (85% yield). VL: 89.05%, AVL: 6.53%; epoxide-δ-valerolactone (EVL): 4.41%; $M_{n,NMR}$: 2972.00 g mol^{-1}.

Synthesis of Nanosponge. Into a 100 mL round-bottom flask equipped with a stir bar, poly(VL-AVL-EVL) and DCM were added. The reaction flask was heated to 46 °C, and 2,2-(ethylenedioxy)bis-(ethylamine) was added dropwise to the stirring solution. The flask was capped with a water-jacketed condenser and stirred. The solvent was removed in a vacuum; the nanosponges were transferred to 10K MWCO dialysis tubing and dialyzed against DCM, then collected, and dried under vacuum (67%). Nanoparticle size (∼70 nm) was confirmed by TEM (Figure S3) and DLS analysis (Figure S4).

Aldehyde Functionalization of Nanosponge. Under an inert N_2 atmosphere, nanosponges were dissolved in a minimal amount of dimethyl sulfoxide. *N*-Succinimidyl *p*-formylbenzoate was added to the solution via a microsyringe, and the reaction was stirred at room temperature. The product was purified by dialysis using 10K MWCO dialysis tubing against DCM. The contents of the dialysis tubing were collected and dried under vacuum (56% yield).

T-Peptide_ACPP Conjugation to Nanosponge. Under an inert N_2 atmosphere, aldehyde-functionalized nanosponge peptide_ACPP were dissolved in minimal *d*-DMSO. 2,2-Dimethoxy-2-phenylacetophenone (DMPA) was added to the reaction mixture via a microsyringe. The solution was irradiated at 365 nm and stirred at room temperature. Peptide conjugation was quantified via reduction in resonance signal of protons associated with an allyl functionality (5.01 and 5.70 ppm) through crude ^{1}H NMR and calculated to be 7.88 peptides per particle as described in eq S1/S2 of the Supporting Information.

Cyanine3 Hydrazide Dye Conjugation to Peptide-Conjugated Nanosponge. Under an inert N_2 atmosphere, peptide-functionalized nanosponges were dissolved in *d*-DMSO. Cyanine3 monohydrazide imaging dye was added to the reaction vial via a syringe, and the reaction was stirred at room temperature in the absence of light. The resulting mixture was purified by dialysis against a 50:50 v/v mixture acetonitrile:MeOH in 10K MWCO dialysis tubing, then diluted in water, and lyophilized to collect a powder (80% yield). Successful attachment of the dye at an equivalence of 9 dye molecules per nanosponge was verified by the absence of the aldehyde peak at 10.20 ppm. The concentrations of the peptide and dye in the fully constructed material were determined to be 243.8 and 281.3 μg mg^{-1} of material, respectively.

https://dx.doi.org/10.1021/acs.chemmater.9b02840
Chem. Mater. 2020, 32, 3707−3714

Scheme 1. Mechanism of Action of the Targeted Nanosponge Drug Delivery System[a]

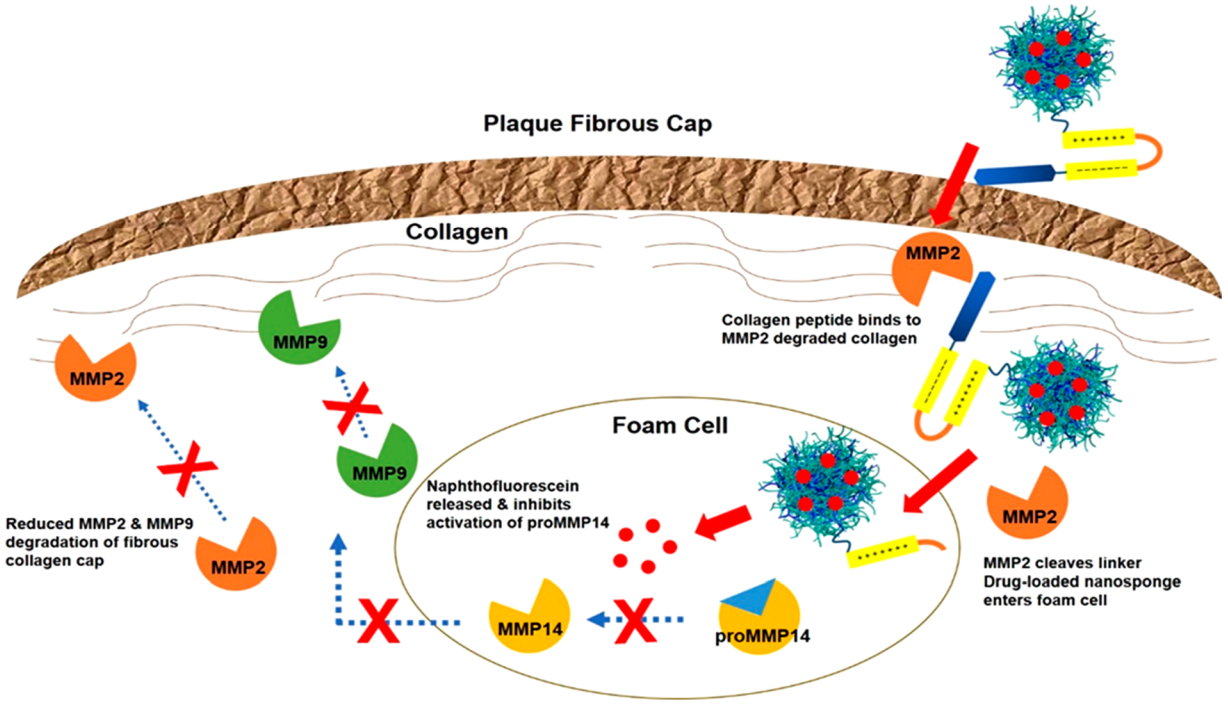

[a]The collagen-homing peptide binds the MMP2-degraded collagen, followed by the cleavage of the peptide linker by MMP2. The cell penetrating polycationic peptide carries the nanosponge into the foam cells, releases the MMP14 conversion inhibitor naphthofluorescein, thereby inhibiting activation of proMMP14 and reducing the levels of plaque destabilizing MMP2 and MMP9 through preventing their activation.

Encapsulation of Naphthofluorescein into Peptide- and Dye-Conjugated Nanosponge. In a conical centrifuge tube, naphthofluorescein along with nanosponges was dissolved in DMSO. The solution was vortexed until a homogeneous solution was achieved. Cell culture water containing 0.1 wt % D-α-tocopherol poly(ethylene glycol) 1000 succinate was added, vortexed, and centrifuged. The supernatant was decanted, and cell culture water was added to the tube and vortexed again. The mixture was centrifuged, the supernatant was decanted, and cell culture water was added. The resulting solution was lyophilized. HPLC analysis (Figure S9) indicated an average drug loading of 23.5 wt %, corresponding to a 94% drug loading efficiency.

T-Peptide_ACPP-Nanosponge Associated Cell Toxicity. A six-well plate was seeded with RAW cells and HT1080 cells and topped up with complete DMEM media. A T-peptide_ACPP-Cy3 labeled nanosponge (1 mg/mL construct concentration) was added per well, and the cells were cultured in a cell incubator at 37 °C for 5 days. Without discarding used media in the wells, adherent cells were scraped gently to dislodge, aspirated, and spun down at 400 rcf for 5 min. Then the supernatant was discarded, and the cell pellet was suspended with fresh DMEM. Cell counting was performed by using a hemocytometer, and 50000 of each type of cell were put into each well on a 96-well plate. After addition of alamarBlue reagent into each well, the microplate was incubated for 2 h at 37 °C. The plate was scanned in a colorimetric plate reader at 570 nm absorbance.

Assay of MMP14 Activity. We used a peptide sequence that is preferentially cleaved by MMP14 to create a FRET probe with N terminal Cy3.5 and C terminal BHQ (Black Hole Quencher). The presence of MMP14 activity will cleave the peptide sequence and separate the Cy3.5 from its BHQ. Cells were dislodged from the flask without the use of trypsin by using a cell scraper. This is to prevent trypsin, a broad-spectrum protease, from digesting the MMP14 FRET peptide indiscriminately. The cells were centrifuged at 4000 rcf for 5 min; the cell pellet was suspended in PBS and counted with a hemocytometer. About 50000 cells were seeded into each test well in a microplate. The microplate was incubated at 37 °C inside a fluorescent microplate reader for 2 h while Cy3.5 signal readings in the (Ex544, Em590) channel were taken every 10 min. The increase in Cy 3.5 signal from time zero to time 120 min is taken as the quantum increase in MMP14 activity on the FRET probe.

Confocal Imaging of Live Cells Treated with Targeted Construct. HT1080 murine fibrosarcoma cells and RAW murine macrophage cells were grown on coverslips with DMEM. Cells were incubated with the targeted nanosponge labeled with Cy3 dye and loaded with naphthofluorescein overnight at 37 °C with 5% CO_2. The next day, cells were counter-stained with Cell Tracker Green for 30 min and Lysotracker Blue and Hoechst 5 min prior to confocal imaging. Fluorescent and transmitted light images were collected by using a Nikon A1r+ confocal microscope equipped with a 60× water immersion objective. Images were collected with the 405, 488, and 568 nm lasers sequentially to minimize bleed-through.

Live Cell Imaging of RAW Cells with Targeted Nanosponges. RAW cells were seeded in an 8-well chambered coverslip overnight and stained with Lysotracker Blue for 30 min and Cell Tracker Green for 10 min prior to three washes with PBS. Cy3-labeled nanosponges were first sonicated for 10 min, mixed with MMP2 at 37 °C, and shaken at 500 rpm for 2 h. The Cy3-labeled nanosponge particles were then added to the culture immediately prior to live imaging. The time-lapse experiments were conducted with a Nikon A1R confocal microscope in resonant scanning mode to prevent photobleaching. Images were collected sequentially by utilizing 405, 488, and 561 nm solid-state lasers. Z-series images were collected at multiple positions by utilizing a motorized XY stage. A Nikon Apo LWD 40× WI, 1.15 NA objective was used.

Blood Clearance and Biodistribution. Mice were housed on a 12 h light/dark cycle with *ad libitum* access to food and water. Male C57Bl6 mice aged 8 weeks were injected with nanosponge through tail veins, and blood samples were taken from the tails at different time points. Blood samples were collected and measured at 800 nm by using an Odyssey infrared imaging system. For biodistribution, organs including heart, spleen, liver, kidney, and lung were collected, and measurements were performed at 800 nm.

Degradation Assay. Nanosponges labeled with NP-Cy7 were dissolved and resuspended in PBS and platelet poor plasma (PPP) at

https://dx.doi.org/10.1021/acs.chemmater.9b02840
Chem. Mater. 2020, 32, 3707−3714

Scheme 2. Synthesis Scheme for the Formation of Peptide-Conjugated, Dye-Labeled, Naphthofluorescein-Loaded Nanosponges

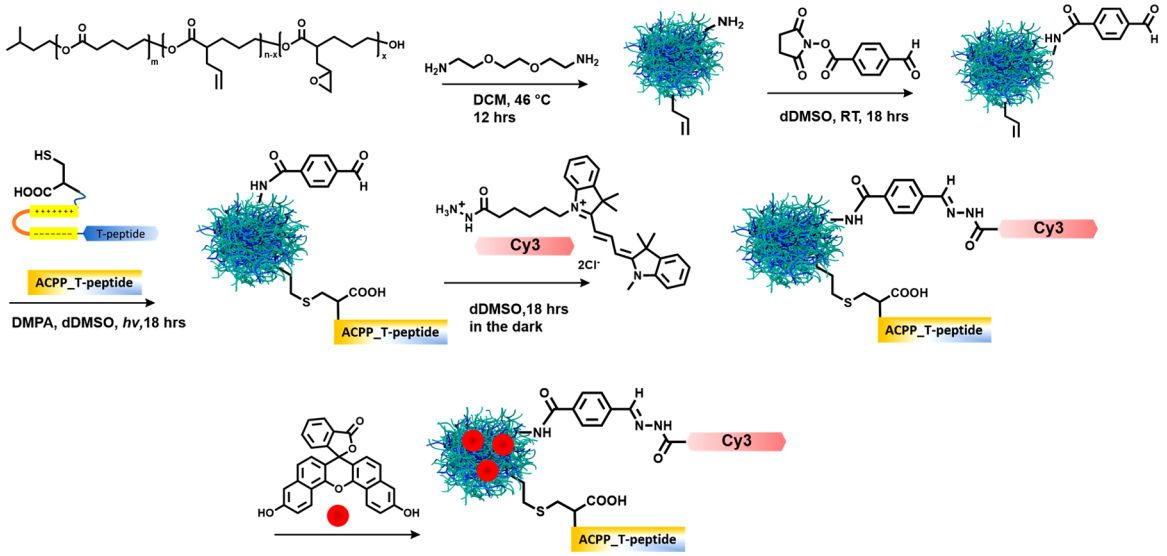

0.7 mg/mL, respectively. The nanosponge solution was incubated under a water bath at 37 °C and centrifuged by using a 10kD spin column at 10K rcf for 10 min. The fluorescence intensity of the supernatant was measured and quantified at 800 nm by using Odyssey infrared imaging system. Triplicate of samples were collected at 1, 4, and 24 h.

Statistical Analysis. All quantitative data are analyzed by PRISM 6 (GraphPad Software Inc.) and reported as mean ± 1 standard deviation. Statistical analysis was performed by using ANOVA followed by Tukey's multiple comparison test, with $p < 0.05$ considered statistically significant.

RESULTS

Collagen is a major component of the extracellular matrix of plaques and forms the structural framework for stability.[36] Plaques are formed within the intima layer of the artery,[37] and collagen IV is present in abundance in the basement membrane of intima cells[38] very close to the plaque, making collagen IV an ideal target. We sought to capitalize on a peptide known to bind to a cryptic epitope on collagen IV exposed through degradative action of MMP2 and investigate its ability as the homing agent for the delivery system.[39] This approach has the ability to provide specific homing and delivery to areas of the plaque with collagen IV, the structural integrity of which has been weakened as a result of MMP2 activity. It was necessary to design a peptide that not only targets but also upon successful binding acts as a cell penetrating unit to shuttle the delivery system effectively into the cell to deliver the MMP inhibitor. As a result, we linked the collagen-homing T-peptide (TLTYTWS) to an activatable cell penetrating peptide (ACPP) that is specifically cleaved by MMP2.[40−42] The ACPP comprises a polycationic sequence of 9 D-arginine zippered to a polyanionic sequence of 8 D-glutamic acid held together by a U-shaped peptide linker (5-amino-3-oxapentanoyl flexible hydrophilic linker) that contains an amino acid sequence of PLGC(Me)AG that is preferentially cleaved by MMP2. In this manner, the ACPP is cleaved at its peptide linker unit and releases the polycationic chain of the D-amino arginine sequence to penetrate cell membranes by its net positivity. If any payload, such as drug loaded particles, is attached to this polycationic arm, it is carried along into cells. Unlike other MMPs, MMP14 activation is an intracellular process that requires furin activation. In an attempt to spare unrelated MMPs, we chose naphthofluorescein as the drug payload for the nanocarrier, a hydrophobic small molecule near-infrared fluorophore that inhibits furin,[43] as a drug to specifically stop MMP14 activation.

With this, the desired nanocarrier required the integration of three functional components—the targeting peptide, imaging dye, and naphthofluorescein MMP14 inhibitor—to achieve plaque-targeting specificity, environment triggered entry of payload into plaque cells, and a controlled delivery of the drug payload (Scheme 1). Conjugating both peptide and imaging dye to the nanosponge surface without compromising the function of either molecule coupled with the complexity and number of functional groups present on the targeting peptide sequence presented synthetic challenges. An orthogonal design was implemented to retain the activity of the peptide and dye and perform a sequential conjugation to orthogonal functionalities integrated to the particle backbone. The nanocarrier was synthesized by following a reported intermolecular cross-linking technique to yield nanoparticles in desired sizes of 60−80 nm.[31] The cross-linking chemistry involves the reaction of linear polyvalerolactone functionalized with pendant allyl and epoxide groups (Scheme 2) with diamine units.[30] The epoxide:amine cross-linking ratio determines the size of the resulting particle and yields a particle with amine and allyl functionalities on the surface as all epoxides have been consumed (Figure S1). This successful reaction was confirmed by NMR spectroscopy analysis (Figure S2) and is in agreement with reported results for the synthesis of these nanosponge materials.[30,33,44−46] Transmission electron microscopy (TEM) and dynamic light scattering (DLS) confirmed the synthesized particle for the planned study to be 70 ± 14 nm (Figures S3 and S4). The solubility of the particle in organic solvents and the ability to follow conjugations to the polymer backbone by NMR spectroscopy make the nanoparticle an ideal candidate for the proposed postmodification chemistries (Scheme 2). For example, the allyl functionality provided a pathway to conjugate the cysteine-functionalized polycationic arm of the

https://dx.doi.org/10.1021/acs.chemmater.9b02840
Chem. Mater. 2020, 32, 3707−3714

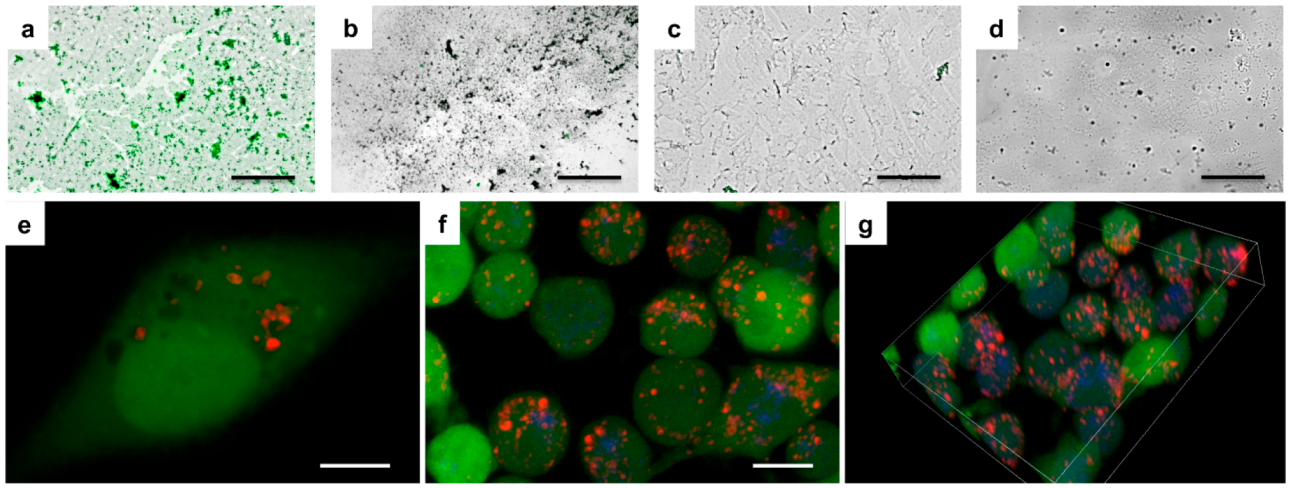

Figure 1. Confirmation of specific binding of FITC collagen peptide to *in vitro* digested collagen. (a) Collagen peptide-FITC binds to MMP2 digested collagen IV. (b) Scrambled peptide-FITC does not bind to MMP2 digested collagen IV. (c) Collagen peptide-FITC does not bind to MMP2 digested collagen IV that was preblocked with nonlabeled collagen peptide. (d) Collagen peptide-FITC does not bind to collagen IV without MMP2 digestion. Scale bar = 500 μm. (e) Confocal image of HT1080 cell uptake of Cy3 (red) labeled nanosponge. Image is taken in the Z stack middle of the cell layer showing intracellular signal. (f) Confocal microscopy of RAW cells to investigate lysosomes location. 2D reconstruction of Z stack confocal images of RAW cells with uptake of Cy3 (red) labeled nanosponge are shown as red dots while the lysosomes are in blue. (g) 3D snapshot showing that the red and blue dots are spatially apart. Scale bar = 8 μm. Representative images for n = 3 are shown.

T-peptide_ACPP sequence through thiol−ene click chemistry.[34]

The attachment of imaging dyes is often achieved by conjugation to amine groups through NHS ester chemistries. However, the T-peptide ACPP sequence contains amine groups, and this attachment chemistry would result in labeling the particle and also the targeting peptide. Off-target dye labeling of the peptide could potentially interfere with peptide confirmation and bioactivity, but it was avoided by strategically transforming the amine functionality into an aldehyde to provide an orthogonal surface unit for the attachment of imaging dyes possessing a hydrazide functionality for conjugation. *N*-Succinimidyl *p*-formylbenzoate was added in an NHS ester reaction to transform amines to aldehyde entities where the selected cyanine3 monohydrazide dye (Cy3) will form a hydrazone bond to exclusively label the surface of the particle (Figure S5 and Scheme 2). The synthetic pathway of the theranostic drug delivery system after nanoparticle formation was performed by first modifying the amine functionality, followed by the attachment of the peptide and then conjugation of the dye to the installed aldehyde functionality as detailed below. In the final step, we loaded the naphthofluorescein into the postmodified particle via a developed nanosolubilization method (see the Supporting Information).

The collagen binding peptide and the ACPP were synthesized by solid phase peptide synthesis and purified by high-performance liquid chromatography (HPLC) (Figure S6). Next, the successful attachment of T-peptide_ACPP to the nanosponges was confirmed via ^{1}H NMR, and quantification was determined via reduction in chemical shift at 5.04 and 5.73 ppm (Figure S7) associated with the allyl protons. The T-peptide_ACPP loading was determined to be 7.88 peptides per particle. For particle tracking *in vitro*, fluorescent cyanine3 monohydrazide (Cy3 dye) was conjugated to the nanosponge surface via aldehyde−hydrazide click chemistry using the previously installed aldehyde moiety. The attachment of the dye to the nanosponge surface was confirmed via absence of the aldehyde chemical shift in the ^{1}H NMR spectra (Figure S8). Lastly, the drug of interest, naphthofluorescein, was loaded by entrapment into the fully functionalized nanosponges conjugated with T-peptide_ACPP and Cy3 dye. Because of the small experimental scale, we did not precipitate the particle into water but rather washed the particle with excess cell culture water during the encapsulation procedure and determined a drug loading of 23 wt % and 94% drug loading efficiency using HPLC detection (Figure S9). The resulting solution was lyophilized to obtain the full construct of peptide-targeted, ACPP-functionalized, drug-loaded, Cy3 fluorescent nanosponges.

To validate the collagen-homing ability of the peptide separately, FITC was conjugated to the peptide, and *in vitro* binding on glass slides coated with MMP2 digested collagen IV was demonstrated (Figure 1a−d). Effective cell penetration of ACPP in the presence but not the absence of active MMP2 was demonstrated (Figure S10) by using the specific hybridization internalization probe (SHIP) technology.[47] We generated an ACPP variant with a C terminal alkyne functional handle for click chemistry. The SHIP technique uses two 20-mer ssDNA sequences, a fluorescent probe (FIP) with a 5′ fluorophore (Cy5), and a 3′ azide that is "clicked" onto the ACPP by using copper-catalyzed azide−alkyne cycloaddition. The FIP-functionalized ACPP was incubated with non-phagocytic similian virus endothelial cells (SVEC4-10) overnight. A quencher probe (QPC) comprising a complementary ssDNA sequence with a 3′ Black Hole Quencher 2 (BHQ2) was then added to the cell culture and incubated for 30 min at 4 °C to hybridize to any extracellular FIP, quenching its fluorescence, while the fluorescence of the internalized FIP is maintained because the QPC cannot access any internalized material.

Next, using the murine fibrosarcoma HT1080 cell line, we investigated cellular uptake of the drug-loaded peptide and dye-conjugated nanosponge construct. HT1080 cells naturally produce MMPs including MMP2.[48] Cells were incubated overnight with the T-peptide_ACPP-nanosponge construct at

https://dx.doi.org/10.1021/acs.chemmater.9b02840
Chem. Mater. 2020, 32, 3707−3714

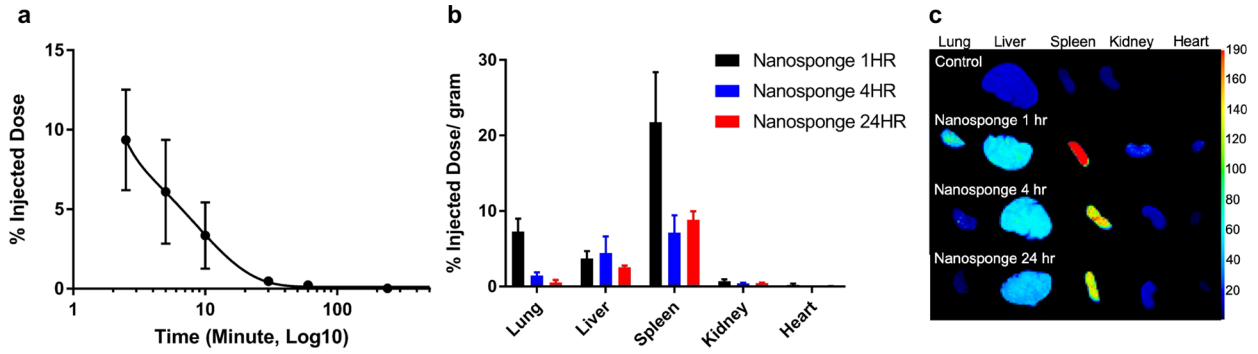

Figure 2. Blood clearance and biodistribution of nanosponge *in vivo*. (a) Circulation time of nanosponge in blood for 24 h. (b) Quantitation of nanosponge accumulated in lung, liver, spleen, kidney, and heart at 1, 4, and 24 h. (c) Accumulation of nanosponge in organs.

37 °C; the cell cytoplasm was stained green the next day and examined with confocal live cell microscopy (Nikon A1) in the FITC and TRITC channels. Figure 1e shows that the construct had been internalized by the cells.

Furthermore, we investigated whether the nanoparticle construct entered lysosomes when incubated with murine macrophage RAW cells which represent our *in vivo* target cells (plaque resident macrophages and foam cells). Murine RAW cells are naturally phagocytic, and they also secrete MMPs, including MMP2. Both cell lines also produce MMP14 which can be efficiently inhibited with naphthofluorescein (Figure S11). By incorporating the ACPP that is cleaved by MMP2, we are in fact creating a nanosponge payload that has a net positive charge from the polycationic D-arginine arm attached to it once the peptide linker of the ACPP is cleaved. In this manner, it provides a way for "lysosomal escape" of the drug-loaded nanosponge by the proton sponge effect,[49] allowing the nanosponge to escape back into the cell cytoplasm through the endosomal membrane, avoiding acid degradation of the nanosponge and drug. After an overnight incubation of the Cy3 conjugated nanoparticle construct with RAW cells, the cell cytoplasm was stained with Cell Tracker Green and Lysotracker Blue/or Hoechst to stain the nucleus (Invitrogen). As shown in Figure 1f,g, we observed no colocalization of the red and blue fluorescent signals in the RAW cells, indicating that the nanoparticle constructs have successfully escaped the cell lysosomes and are not associated or have entered the nucleus (Figure S12). We also witnessed the internalization of nanosponge particles at 15 min after the particles had been in contact with RAW cells in culture (Figure S13). We also demonstrated that the nanosponges were nontoxic to both cell lines (Figure S14) before testing the material *in vivo*.

Nanoparticle drug delivery systems may be diverted from their target due to uptake by macrophage cells during blood circulation,[50] depositing them in the liver and spleen. To investigate this, we performed *in vivo* biodistribution experiments as well as *in vitro* stability testing. As shown in Figure 2a, 9.35% of the injected nanosponges were still detected in the blood after 2.5 min, which dropped down to 0.5% after 30 min, showing a long enough blood circulation to reach the biological target *in vivo*. One hour after the tail injection, 21.8% of the nanosponges accumulated in the spleen, 7.3% in the lung, 3.7% in the liver, and negligible amounts in the kidney and heart (Figure 2b). The high lung uptake is likely an unspecific entrapment which is only seen at this early time point. By 4 h, the accumulated nanosponges dropped to 7.1% in the spleen, 1.4% in the lung, and similar amounts in the liver, kidney, and heart compared to 1 h. In the following 24 h after injection, most accumulated nanosponges were cleared from the organs including lung, kidney, heart, and liver, and only 8% were left in the spleen (Figure 2b,c). The results indicated that most of nanosponges were sequestrated in the spleen and cleared within 24 h. To investigate the degradation profile in buffer and plasma, we incubated the nanosponges in phosphate-buffered saline (PBS) and platelet poor plasma (PPP), respectively, and filtered the supernatant at different time points including 0, 1, 4, and 24 h. No fluorescence was observed in the supernatant, indicating there was no degradation of the nanosponge and confirming good stability over 24 h (Figures S15 and S16).

In summary, we demonstrated the generation of peptide-labeled and drug-loaded nanosponges targeted toward MMP2-degraded collagen IV as seen in unstable plaques with the potential ability to enhance the collagen content of plaques through delivery of nanosponge drug cargo. Our study paves the way for future translational work on peptide-directed nanotechnology in biological applications, and our designed construct presents great potential for the development of biological targeted drug delivery therapeutics in humans for the prevention of heart attacks.

■ ASSOCIATED CONTENT

Supporting Information

The Supporting Information is available free of charge at https://pubs.acs.org/doi/10.1021/acs.chemmater.9b02840.

Expanded version of the Experimental Section; experimental details including materials, synthesis of drug-loaded nanosponges, confocal imaging experiments, *in vitro* experiments, and instrumentation (PDF)

■ AUTHOR INFORMATION

Corresponding Authors

Christoph E. Hagemeyer − *Vascular Biotechnology Laboratory, Baker Heart and Diabetes Institute, Melbourne, Victoria, Australia; NanoBiotechnology Laboratory, Australian Centre for Blood Diseases, Monash University, Melbourne, Australia;* orcid.org/0000-0002-7114-4023; Email: christoph.hagemeyer@monash.edu

Eva Harth − *Department of Chemistry, University of Houston, Center of Excellence in Polymer Chemistry, Houston, Texas 77024, United States;* orcid.org/0000-0001-5553-0365; Email: harth@uh.edu

https://dx.doi.org/10.1021/acs.chemmater.9b02840
Chem. Mater. 2020, 32, 3707−3714

Authors

Ting-Yi Wang − *NanoBiotechnology Laboratory, Australian Centre for Blood Diseases, Monash University, Melbourne, Australia*

Laken L. Kendrick-Williams − *Department of Chemistry, University of Houston, Center of Excellence in Polymer Chemistry, Houston, Texas 77024, United States; Department of Chemistry, Vanderbilt University, Nashville, Tennessee 37235, United States*

Mei Y. Choy − *Vascular Biotechnology Laboratory, Baker Heart and Diabetes Institute, Melbourne, Victoria, Australia*

Kelly A. Gilmore − *Department of Chemistry, Vanderbilt University, Nashville, Tennessee 37235, United States*

Thomas Bonnard − *NanoBiotechnology Laboratory, Australian Centre for Blood Diseases, Monash University, Melbourne, Australia; INSERM, INSERM UMR-S U1237, Physiopathology and Imaging of Neurological Disorders, University of Caen Normandy, Caen, France*

Hannah A. Pearce − *NanoBiotechnology Laboratory, Australian Centre for Blood Diseases, Monash University, Melbourne, Australia*

Lok Soon Law − *Vascular Biotechnology Laboratory, Baker Heart and Diabetes Institute, Melbourne, Victoria, Australia*

Iska Carmichael − *Monash Micro Imaging, Melbourne, Australia*

Stephen H. Cody − *Monash Micro Imaging, Melbourne, Australia*

Karen Alt − *Vascular Biotechnology Laboratory, Baker Heart and Diabetes Institute, Melbourne, Victoria, Australia; NanoBiotechnology Laboratory, Australian Centre for Blood Diseases, Monash University, Melbourne, Australia*

Complete contact information is available at: https://pubs.acs.org/10.1021/acs.chemmater.9b02840

Author Contributions

T.-Y.W. and L.L.K.-W. contributed equally to this work.

Notes

The authors declare no competing financial interest.

■ ACKNOWLEDGMENTS

L.L.K.-W. acknowledges support from the National Science Foundation Graduate Research Fellowship Program (NSF GRFP DGE-1445197). E.H. and L.L.K.-W. thank the Robert A. Welch Foundation for generous support of this research (#H-E-0041) through the UH Center of Excellence in Polymer Chemistry (CEPC). This work was funded by the National Health and Medical Research Council (NHMRC) as well as the CASS foundation. K.A. was supported by the German Research Foundation. C.E.H. was a National Heart Foundation Career Development Fellow. The work was also supported in part by the National Science Foundation (NSF CHE-1808664), the Juvenile Diabetes Foundation (JDRF 17-2013-324) and the Victorian Government's Operational Infrastructure Support Program.

■ REFERENCES

(1) Go, A. S.; Mozaffarian, D.; Roger, V. L.; Benjamin, E. J.; Berry, J. D.; Blaha, M. J.; Dai, S.; Ford, E. S.; Fox, C. S.; Franco, S.; Fullerton, H. J.; Gillespie, C.; Hailpern, S. M.; Heit, J. A.; Howard, V. J.; Huffman, M. D.; Judd, S. E.; Kissela, B. M.; Kittner, S. J.; Lackland, D. T.; Lichtman, J. H.; Lisabeth, L. D.; Mackey, R. H.; Magid, D. J.; Marcus, G. M.; Marelli, A.; Matchar, D. B.; McGuire, D. K.; Mohler, E. R.; Moy, C. S.; Mussolino, M. E.; Neumar, R. W.; Nichol, G.; Pandey, D. K.; Paynter, N. P.; Reeves, M. J.; Sorlie, P. D.; Stein, J.; Towfighi, A.; Turan, T. N.; Virani, S. S.; Wong, N. D.; Woo, D.; Turner, M. B. Heart Disease and Stroke Statistics—2014 Update: A Report From the American Heart Association. *Circulation* **2014**, *129* (3), e28−e292.

(2) Lafont, A. Basic aspects of plaque vulnerability. *Br. Heart J.* **2003**, *89* (10), 1262−1267.

(3) Schneider, F.; Sukhova, G. K.; Aikawa, M.; Canner, J.; Gerdes, N.; Tang, S.-M. T.; Shi, G.-P.; Apte, S. S.; Libby, P. Matrix Metalloproteinase-14 Deficiency in Bone Marrow−Derived Cells Promotes Collagen Accumulation in Mouse Atherosclerotic Plaques. *Circulation* **2008**, *117* (7), 931.

(4) Suh, W. M.; Seto, A. H.; Margey, R. J. P.; Cruz-Gonzalez, I.; Jang, I.-K. Intravascular Detection of the Vulnerable Plaque. *Circ.: Cardiovasc. Imaging* **2011**, *4* (2), 169.

(5) Johnson, J. L.; Sala-Newby, G. B.; Ismail, Y.; Aguilera, C. M.; Newby, A. C. Low Tissue Inhibitor of Metalloproteinases 3 and High Matrix Metalloproteinase 14 Levels Defines a Subpopulation of Highly Invasive Foam-Cell Macrophages. *Arterioscler., Thromb., Vasc. Biol.* **2008**, *28* (9), 1647−1653.

(6) Sato, H.; Takino, T.; Okada, Y.; Cao, J.; Shinagawa, A.; Yamamoto, E.; Seiki, M. A matrix metalloproteinase expressed on the surface of invasive tumour cells. *Nature* **1994**, *370*, 61.

(7) Ohuchi, E.; Imai, K.; Fujii, Y.; Sato, H.; Seiki, M.; Okada, Y. Membrane Type 1 Matrix Metalloproteinase Digests Interstitial Collagens and Other Extracellular Matrix Macromolecules. *J. Biol. Chem.* **1997**, *272* (4), 2446−2451.

(8) Rosenbaum, E.; Zahurak, M.; Sinibaldi, V.; Carducci, M. A.; Pili, R.; Laufer, M.; DeWeese, T. L.; Eisenberger, M. A. Marimastat in the Treatment of Patients with Biochemically Relapsed Prostate Cancer: A Prospective Randomized, Double-Blind. *Clin. Cancer Res.* **2005**, *11* (12), 4437.

(9) Coussens, L. M.; Fingleton, B.; Matrisian, L. M. Matrix Metalloproteinase Inhibitors and Cancer—Trials and Tribulations. *Science* **2002**, *295* (5564), 2387−2392.

(10) Johnson, J. L.; Fritsche-Danielson, R.; Behrendt, M.; Westin-Eriksson, A.; Wennbo, H.; Herslof, M.; Elebring, M.; George, S. J.; McPheat, W. L.; Jackson, C. L. Effect of broad-spectrum matrix metalloproteinase inhibition on atherosclerotic plaque stability. *Cardiovasc. Res.* **2006**, *71* (3), 586−595.

(11) Johnson, J. L. Matrix metalloproteinases: influence on smooth muscle cells and atherosclerotic plaque stability. *Expert Rev. Cardiovasc. Ther.* **2007**, *5* (2), 265−282.

(12) Richardson, J. J.; Choy, M. Y.; Guo, J.; Liang, K.; Alt, K.; Ping, Y.; Cui, J.; Law, L. S.; Hagemeyer, C. E.; Caruso, F. Polymer Capsules for Plaque-Targeted In Vivo Delivery. *Adv. Mater.* **2016**, *28* (35), 7703−7707.

(13) Ankri, R.; Leshem-Lev, D.; Lev, E. I.; Motiei, M.; Hochhauser, E.; Fixler, D. Gold nanoparticles based imaging technique and drug delivery for the detection and treatment of atherosclerotic vascular disease, *Proc. SPIE 9721*, Nanoscale Imaging, Sensing, and Actuation for Biomedical Applications XIII, **2016**, 97210F-9.

(14) Wei, X.; Ying, M.; Dehaini, D.; Su, Y.; Kroll, A. V.; Zhou, J.; Gao, W.; Fang, R. H.; Chien, S.; Zhang, L. Nanoparticle functionalization with platelet membrane enables multifactored biological targeting and detection of atherosclerosis. *ACS Nano* **2018**, *12* (1), 109−116.

(15) Rink, J. S.; Sun, W.; Misener, S.; Wang, J.-J.; Zhang, Z. J.; Kibbe, M. R.; Dravid, V. P.; Venkatraman, S.; Thaxton, C. S. Nitric oxide-delivering high-density lipoprotein-like nanoparticles as a biomimetic nanotherapy for vascular diseases. *ACS Appl. Mater. Interfaces* **2018**, *10* (8), 6904−6916.

(16) Nandwana, V.; Ryoo, S.-R.; Kanthala, S.; McMahon, K. M.; Rink, J. S.; Li, Y.; Venkatraman, S. S.; Thaxton, C. S.; Dravid, V. P. High-density lipoprotein-like magnetic nanostructures (HDL-MNS): theranostic agents for cardiovascular disease. *Chem. Mater.* **2017**, *29* (5), 2276−2282.

(17) Wickline, S. A.; Neubauer, A. M.; Winter, P. M.; Caruthers, S. D.; Lanza, G. M. Molecular imaging and therapy of atherosclerosis

with targeted nanoparticles. *J. Magn. reson. Imaging* **2007**, *25* (4), 667−680.
(18) Nagavarma, B.; Yadav, H. K.; Ayaz, A.; Vasudha, L.; Shivakumar, H. Different techniques for preparation of polymeric nanoparticles-a review. *Asian J. Pharm. Clin. Res.* **2012**, *5* (3), 16−23.
(19) Panyam, J.; Labhasetwar, V. Biodegradable nanoparticles for drug and gene delivery to cells and tissue. *Adv. Drug Delivery Rev.* **2003**, *55* (3), 329−347.
(20) Soppimath, K. S.; Aminabhavi, T. M.; Kulkarni, A. R.; Rudzinski, W. E. Biodegradable polymeric nanoparticles as drug delivery devices. *J. Controlled Release* **2001**, *70* (1), 1−20.
(21) Rosenblum, D.; Joshi, N.; Tao, W.; Karp, J. M.; Peer, D. Progress and challenges towards targeted delivery of cancer therapeutics. *Nat. Commun.* **2018**, *9* (1), 1410−1422.
(22) Wang, A. Z.; Langer, R.; Farokhzad, O. C. Nanoparticle Delivery of Cancer Drugs. *Annu. Rev. Med.* **2012**, *63* (1), 185−198.
(23) Islam, M. A.; Barua, S.; Barua, D. A multiscale modeling study of particle size effects on the tissue penetration efficacy of drug-delivery nanoparticles. *BMC Syst. Biol.* **2017**, *11* (1), 113.
(24) Ta, H. T.; Truong, N. P.; Whittaker, A. K.; Davis, T. P.; Peter, K. The effects of particle size, shape, density and flow characteristics on particle margination to vascular walls in cardiovascular diseases. *Expert Opin. Drug Delivery* **2018**, *15* (1), 33−45.
(25) Gaumet, M.; Vargas, A.; Gurny, R.; Delie, F. Nanoparticles for drug delivery: The need for precision in reporting particle size parameters. *Eur. J. Pharm. Biopharm.* **2008**, *69* (1), 1−9.
(26) Hoshyar, N.; Gray, S.; Han, H.; Bao, G. The effect of nanoparticle size on in vivo pharmacokinetics and cellular interaction. *Nanomedicine (London, U. K.)* **2016**, *11* (6), 673−92.
(27) Blanco, E.; Shen, H.; Ferrari, M. Principles of nanoparticle design for overcoming biological barriers to drug delivery. *Nat. Biotechnol.* **2015**, *33* (9), 941−51.
(28) Babu, A.; Templeton, A. K.; Munshi, A.; Ramesh, R. Nanoparticle-Based Drug Delivery for Therapy of Lung Cancer: Progress and Challenges. *J. Nanomater.* **2013**, *2013*, 1−11.
(29) Shang, L.; Nienhaus, K.; Nienhaus, G. U. Engineered nanoparticles interacting with cells: size matters. *J. Nanobiotechnol.* **2014**, *12*, 5−16.
(30) Passarella, R. J.; Spratt, D. E.; van der Ende, A. E.; Phillips, J. G.; Wu, H.; Sathiyakumar, V.; Zhou, L.; Hallahan, D. E.; Harth, E.; Diaz, R. Targeted Nanoparticles That Deliver a Sustained, Specific Release of Paclitaxel to Irradiated Tumors. *Cancer Res.* **2010**, *70* (11), 4550−4559.
(31) van der Ende, A. E.; Kravitz, E. J.; Harth, E. Approach to Formation of Multifunctional Polyester Particles in Controlled Nanoscopic Dimensions. *J. Am. Chem. Soc.* **2008**, *130* (27), 8706−8713.
(32) Hariri, G.; Edwards, A. D.; Merrill, T. B.; Greenbaum, J. M.; van der Ende, A. E.; Harth, E. Sequential Targeted Delivery of Paclitaxel and Camptothecin Using a Cross-Linked "Nanosponge" Network for Lung Cancer Chemotherapy. *Mol. Pharmaceutics* **2014**, *11* (1), 265−275.
(33) van der Ende, A. E.; Sathiyakumar, V.; Diaz, R.; Hallahan, D. E.; Harth, E. Linear release nanoparticle devices for advanced targeted cancer therapies with increased efficacy. *Polym. Chem.* **2010**, *1* (1), 93.
(34) van der Ende, A.; Croce, T.; Hamilton, S.; Sathiyakumar, V.; Harth, E. Tailored polyester nanoparticles: post-modification with dendritic transporter and targeting units via reductive amination and thiol-ene chemistry. *Soft Matter* **2009**, *5* (7), 1417−1425.
(35) Lockhart, J. N.; Stevens, D. M.; Beezer, D. B.; Kravitz, A.; Harth, E. Dual drug delivery of tamoxifen and quercetin: Regulated metabolism for anticancer treatment with nanosponges. *J. Controlled Release* **2015**, *220*, 751−757.
(36) Katsuda, S.; Okada, Y.; Minamoto, T.; Oda, Y.; Matsui, Y.; Nakanishi, I. Collagens in human atherosclerosis. Immunohistochemical analysis using collagen type-specific antibodies. *Arterioscler. Thromb.* **1992**, *12* (4), 494−502.
(37) Libby, P.; Ridker, P. M.; Hansson, G. K. Progress and challenges in translating the biology of atherosclerosis. *Nature* **2011**, *473*, 317.
(38) LeBleu, V. S.; MacDonald, B.; Kalluri, R. Structure and Function of Basement Membranes. *Exp. Biol. Med.* **2007**, *232* (9), 1121−1129.
(39) Mueller, J.; Gaertner, F. C.; Blechert, B.; Janssen, K.-P.; Essler, M. Targeting of Tumor Blood Vessels: A Phage-Displayed Tumor-Homing Peptide Specifically Binds to Matrix Metalloproteinase-2-Processed Collagen IV and Blocks Angiogenesis. *Mol. Cancer Res.* **2009**, *7* (7), 1078−1085.
(40) Jiang, T.; Olson, E. S.; Nguyen, Q. T.; Roy, M.; Jennings, P. A.; Tsien, R. Y. Tumor imaging by means of proteolytic activation of cell-penetrating peptides. *Proc. Natl. Acad. Sci. U. S. A.* **2004**, *101* (51), 17867−17872.
(41) Olson, E. S.; Jiang, T.; Aguilera, T. A.; Nguyen, Q. T.; Ellies, L. G.; Scadeng, M.; Tsien, R. Y. Activatable cell penetrating peptides linked to nanoparticles as dual probes for in vivo fluorescence and MR imaging of proteases. *Proc. Natl. Acad. Sci. U. S. A.* **2010**, *107* (9), 4311−4316.
(42) Olson, E. S.; Whitney, M. A.; Friedman, B.; Aguilera, T. A.; Crisp, J. L.; Baik, F. M.; Jiang, T.; Baird, S. M.; Tsimikas, S.; Tsien, R. Y.; Nguyen, Q. T. In vivo fluorescence imaging of atherosclerotic plaques with activatable cell-penetrating peptides targeting thrombin activity. *Integr. Biol.* **2012**, *4* (6), 595−605.
(43) Jiao, G.-S.; Cregar, L.; Wang, J.; Millis, S. Z.; Tang, C.; O'Malley, S.; Johnson, A. T.; Sareth, S.; Larson, J.; Thomas, G. Synthetic small molecule furin inhibitors derived from 2,5-dideoxystreptamine. *Proc. Natl. Acad. Sci. U. S. A.* **2006**, *103* (52), 19707−19712.
(44) Subramanian, S.; Anandam, S.; Kannan, K.; Rajappan, M. Nanosponges: A Novel Class of Drug Delivery System - Review. *J. Pharm. Pharm. Sci.* **2012**, *15*, 103−11.
(45) Lockhart, J. N.; Stevens, D. M.; Beezer, D. B.; Kravitz, A.; Harth, E. Dual drug delivery of tamoxifen and quercetin: Regulated metabolism for anticancer treatment with nanosponges. *J. Controlled Release* **2015**, *220*, 751−757.
(46) Stevens, D. M.; Gilmore, K. A.; Harth, E. An assessment of nanosponges for intravenous and oral drug delivery of BCS class IV drugs: Drug delivery kinetics and solubilization. *Polym. Chem.* **2014**, *5* (11), 3551−3554.
(47) Liu, H.; Johnston, A. P. R. A Programmable Sensor to Probe the Internalization of Proteins and Nanoparticles in Live Cells. *Angew. Chem., Int. Ed.* **2013**, *52* (22), 5744−5748.
(48) Stanton, H.; Gavrilovic, J.; Atkinson, S. J.; d'Ortho, M. P.; Yamada, K. M.; Zardi, L.; Murphy, G. The activation of ProMMP-2 (gelatinase A) by HT1080 fibrosarcoma cells is promoted by culture on a fibronectin substrate and is concomitant with an increase in processing of MT1-MMP (MMP-14) to a 45 kDa form. *J. Cell Sci.* **1998**, *111* (18), 2789−2798.
(49) Khalil, I. A.; Kogure, K.; Akita, H.; Harashima, H. Uptake Pathways and Subsequent Intracellular Trafficking in Nonviral Gene Delivery. *Pharmacol. Rev.* **2006**, *58* (1), 32−45.
(50) Moghimi, S. M.; Szebeni, J. Stealth liposomes and long circulating nanoparticles: critical issues in pharmacokinetics, opsonization and protein-binding properties. *Prog. Lipid Res.* **2003**, *42* (6), 463−478.

https://dx.doi.org/10.1021/acs.chemmater.9b02840
Chem. Mater. 2020, 32, 3707−3714